ACSNANO
www.acsnano.org
ARTICLE

Fe on Sb(111): Potential Two-Dimensional Ferromagnetic Superstructures

Yinghui Yu,[†,⊥] Huixia Fu,[§,⊥] Limin She,[†,#,⊥] Shuangzan Lu,[†] Qinmin Guo,[†] Hui Li,[*,§] Sheng Meng,[§] and Gengyu Cao[*,†]

[†]State Key Laboratory of Magnetic Resonance and Atomic and Molecular Physics, Wuhan Institute of Physics and Mathematics, Chinese Academy of Sciences, Wuhan 430071, China

[§]Institute of Physics, Chinese Academy of Sciences, Beijing 100190, China

Supporting Information

ABSTRACT: **It is highly desirable to fabricate two-dimensional ferromagnetic membranes based on orthodox magnetic elements because of their inherent magnetic properties. In this work, we report on two superstructures including a honeycomb-like lattice and identical nanocluster arrays formed by depositing Fe on Sb(111). Combined with first-principles calculations, both detailed atomic structures have been clarified. The honeycomb structure consists of a single layered Fe−Sb phase, and the cluster phase is assigned as a (3 × 3) Fe_3Sb_7 superlattice. Both structural phases exhibit high magnetic moments localized on *d* bands of Fe. Our results provide a method to fabricate 2D magnetic superstructures possessing great potential in the realization of the Haldane model, spintronics applications, and single atom catalysis.**

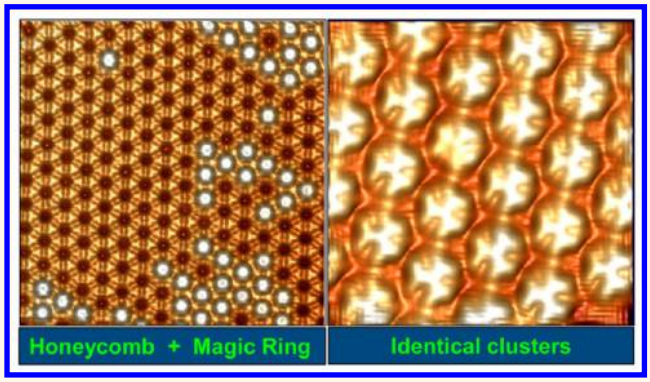

KEYWORDS: *honeycomb lattice, identical cluster, Sb(111), scanning tunneling microscopy*

Nanostructures with controllable magnetism have been recently intensively studied because they are valuable models to study fundamental magnetic phenomena,[1] and also urgently needed in many industrial fields, such as information process and storage, catalyst, energy applications, and permanent magnets.[2] Among various magnetic nanostructures, the two-dimensional (2D) magnet is the most impressive one. It is theoretically predicted to exhibit specific long-range magnetic order, leading to extremely rich physical and chemical properties and being applicable in spintronic devices.[3−12] In 1988, Haldane proposed that the 2D honeycomb magnetic structure can present a nonzero quantization of the Hall conductance due to the "parity anomaly",[13] which provides the conceptual basis for exploring topological insulators and superconductors.[14−18] Although the topological Haldane model has been experimentally realized by ultracold Fermionic atoms in an optical honeycomb lattice in 2014,[19] researchers are still trying hard to look for more stable and easy-to-grow materials, especially atomic-thick 2D ferromagnetic material, to realize this model. Until now, to our best knowledge, successful fabrication of a 2D ferromagnet is still very rare in experiments, although hydrogenated graphene and its analogues,[3−5] hole-doping monolayer GaSe,[6,7] and layered transition metal dichalocogenides[8−12] have been proposed to realize 2D magnets. Recently, hafnene (atomic Hf layer) with a metallic and spin-polarized electronic structure was obtained by annealing transition metal Hf deposited Ir(111),[20] indicating that the metal adlayer can be a good candidate for a 2D magnet. On the other hand, as orthodox magnetic elements, Fe- and Co-based low-dimensional structures can be another effective way to realize 2D magnetism. As early as 2000, Izquierdo *et al.* already predicted that a 2D Fe membrane is provided with a much higher magnetic moment and larger magnetic anisotropy compared to its bulk counterpart.[1] Recently, Zhao *et al.* successfully grew the monatomic Fe layer in perforations of graphene but with the square lattice.[21] However, the honeycomb membrane of Fe-based materials, which should possess similar properties to magnetic graphene-like materials and be worthy of exploring the Haldane model, is still highly desirable but not experimentally realized yet.

In this article, we report that 2D Fe-based superstructures can be fabricated on a Sb(111) surface. Using scanning tunneling microscopy (STM), we systematically investigated the configurations of the Fe/Sb adlayer. We clarify that two

Received: December 13, 2016
Accepted: January 10, 2017
Published: January 10, 2017

DOI: 10.1021/acsnano.6b08347
ACS Nano 2017, 11, 2143−2149

types of superstructural phases (hereafter referred as phase A and B) can simultaneously form on Fe-deposited Sb(111). Combined with the first-principles calculations, phase A is characterized as a bilayer Fe−Sb alloy structure with a topmost magic ring superstructure and an underlying (4 × 4) honeycomb lattice. Phase B exhibits a (3 × 3) identical nanocluster array with a Fe_3Sb_7 phase in each cluster. The calculations demonstrate that the Fe−Sb surface alloy is provided with both honeycomb periodic structure and high magnetic moments (2.0−3.0 μB/Fe), so that it can be a good material for realizing the Haldane model. In addition, the identical magnetic moment of Fe atoms in bilayer Fe−Sb alloy to isolated Fe indicates that such superstructure has also great application potential in single atom catalysis.[22,23]

RESULTS AND DISCUSSION

Figure 1 is a typical STM image of an as-prepared sample with coverage of about 0.2 ML. Two ordered structural phases

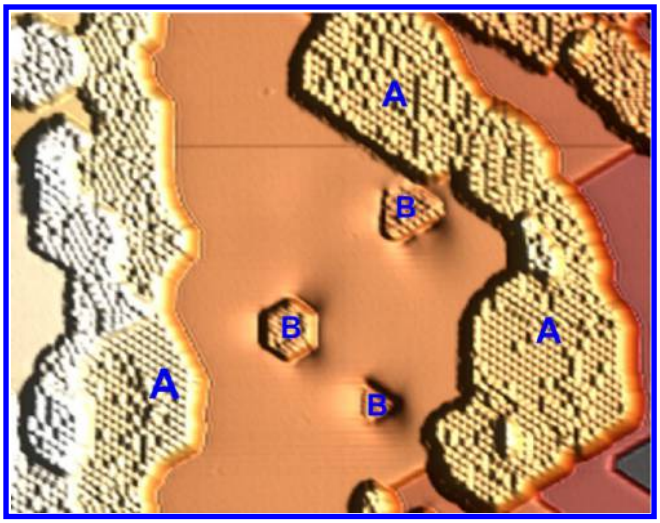

Figure 1. STM image of Fe deposited on Sb(111). Two ordered structural phases (labeled A and B) formed on the surface. (128 nm × 100 nm, U = 1.5 V, I = 0.6 nA).

labeled with A and B form at different surface regions. The area of phase A exists as an irregular shape with a bilayer structure. This structural phase can grow across the step edge and extend into the lower terrace of Sb(111). The phase B region emerges as a truncated triangular shape with a small size and exhibits a single layer structure composing of close-packed protrusions. Both phases can coexist on the substrate surface within annealing temperatures ranging from 480 to 600 K at any coverage ranging from 0.1 to 1.0 ML, implying that both phases have similar formation energy and high stability. With the Fe coverage increasing, phase A can spread over to a large area of the surface, while the phase B area shows little extension still with a truncated triangular shape. Both phases can also be obtained by annealing Sb(111) with Fe deposited at room temperature (Figure S1, Supporting Information). However, compared with the case of Fe deposition at high substrate temperatures, phase A exhibits many islands with small sizes.

Honeycomb Lattice of Fe−Sb Surface Alloy. Figure 2a shows a close look at the phase A that can be viewed as a bilayer film growing across a substrate step edge. The whole surface shows no height difference at both step sides, implying the existence of more than one bilayer at the lower terrace. The topmost layer consists of identical protrusions with a hexagonal shape. The underlying layer of phase A exhibits a corner hole surrounded by six close-packed atomic arrays, a characteristic signature of a honeycomb lattice. Figure 2b shows a simultaneous atomic resolution STM image of the substrate and phase A. Here we can clearly identify the topmost protrusions as identical nanoring and the underlying layer as a typical honeycomb lattice. The apparent height of the bilayer is about 2.5 Å relative to the Sb(111) terrace (Figure S2a, Supporting Information). It is noted that a bilayer island with an irregular shape can be formed on top of the identical nanoring, as shown in Figure 2b. Its apparent height is ∼4.1 Å, consistent with that of the substrate step and larger than that of the underlying bilayer (Figure S2b,d, Supporting Information). Thus, it is straightforward that the island in Figure 2a contains one and two bilayers formed on the upper and lower substrate terraces, respectively. Hence, the whole phase A surface shows no height difference at both step sides.

Figure 2 panels c and d show the STM image recorded at the area of the honeycomb lattice. We can clearly distinguish each identical close-packed atomic array as an equilateral-triangle shape with atoms locating at the vertexes and central line. Every two adjacent atomic arrays mirror each other, corresponding to the A and B interpenetrating sublattices of graphene-like materials. Furthermore, the single protrusion with a hexagonal shape resides at the top of a corner hole of the honeycomb lattice (Figure 2d), identified as a "magic" ring as discussed below. Figure 2e shows a zoomed-in STM image in which the bilayer structure is clearly resolved. It is noted that those topmost bright protrusions indeed consist of six atoms arranging as a regular hexagonal configuration. A height profile recorded along the packing orientations (Figure 2f) indicates that the periodicities of the honeycomb lattice and the magic ring are ∼17.2 Å, exactly four times that of the lattice constant of Sb(111) (4.3 Å). Therefore, phase A can be characterized as topmost (4 × 4) ring and underlying (4 × 4) honeycomb reconstructions with respect to the (1 × 1) lattice of Sb(111). Both structures can be viewed as "magic mismatched" systems, since the periodicities of constructions actually equal four times that of the lattice constant of Sb(111).

By superimposing the substrate lattice in parallel on an atomic resolution STM image (Figure 2g), we reveal that vertex and center atoms in each triangle-shaped atomic array (A and B sublattices) locate at the hollow sites of the underlying Sb(111). Six atoms in each magic ring just reside on the top sites of the underlying corner hole and the neighboring magic rings are spaced by a distance as long as four times that of the Sb(111) lattice constant, which is consistent with the results measured in Figure 2f. Furthermore, the orientation of the honeycomb lattice is found to be well linked with the relative close-packed [1−10] direction of the substrate lattice. It is further proven by the fast Fourier transform of Figure 2b where the reflexes of the honeycomb lattice rotate by 30° in comparison with those of the Sb(111) lattice. However, the packing sequence of the topmost (4 × 4) magic ring array can be broken by some irregular distortion of the underlying honeycomb lattice (marked by yellow circles in Figure 2g) which could be caused by the substrate defects.

To gain a deeper understanding of the growth mode of phase A, we focus on the square region highlighted in Figure 2b. Figure 2h shows the simultaneous atomic resolution of the topmost island and the supporting bilayer film. This island displays the same bilayer configuration and packing orientation

DOI: 10.1021/acsnano.6b08347
ACS Nano 2017, 11, 2143−2149

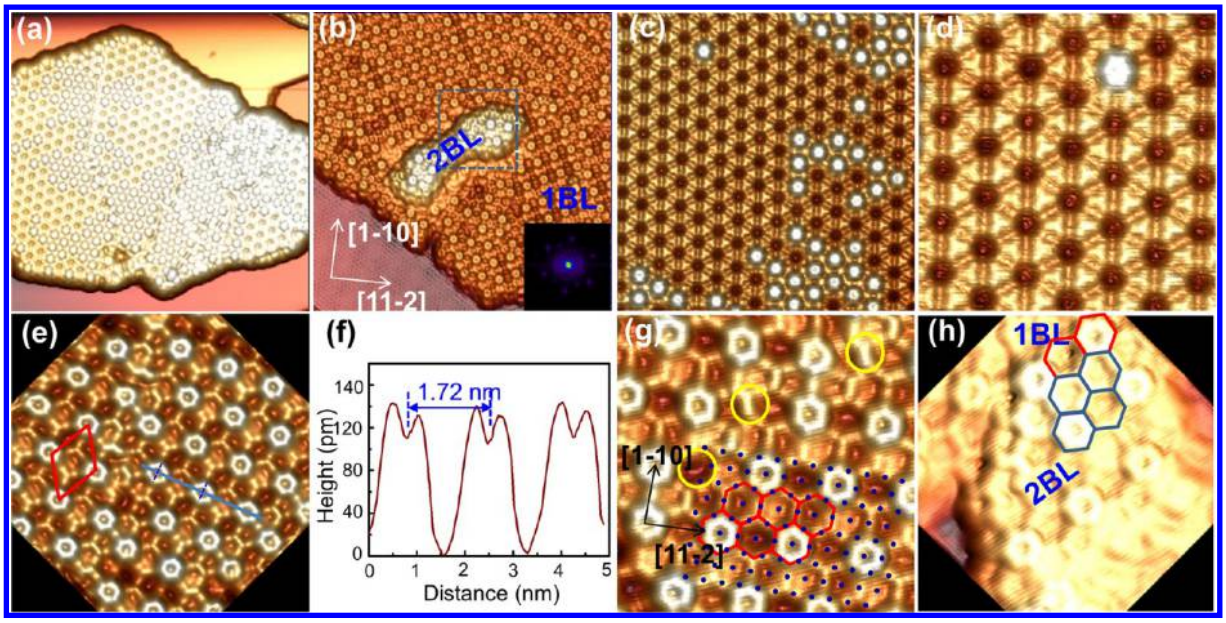

Figure 2. (a) STM topography recorded in the region of phase A that grows across the step edge of Sb(111). The bilayer structure of phase A is resolved (41.3 nm × 41.3 nm). (b) STM image of the bilayer region. Two bilayers are labeled with 1BL and 2BL, respectively. The inset shows the corresponding fast Fourier transform (29.3 nm × 29.3 nm). (c) Zoom-in STM image of the bilayer of phase A (22.4 nm × 22.4 nm). (d) Zoom-in STM image of the honeycomb structure. The bright protrusion corresponds to the "magic" ring of the second layer (10.3 nm × 10.3 nm). (e) STM topography on the "magic" rings. The rhombus denotes the unit cell (10.9 nm × 10.9 nm). (f) A height profile taken along the blue line in (e). (g) Zoom-in STM image on the "magic" rings. The Sb(111) lattice (blue dots) is superimposed. The underlying structure is highlighted by red honeycomb patterns and the yellow circles denote the defects (7 nm × 7 nm). (h) STM image recorded at the square area of panel b where two bilayers are simultaneously resolved. The first-bilayer and second-bilayer honeycombs are highlighted by red and blue colors, respectively (7 nm × 7 nm). All STM images are recorded under U = 0.4 V and I = 0.4 nA.

as the underlying layers. By analysis of the atomic packing sequence near the island edge, we find that atoms of the bilayer island exactly locate on the top sites of the underlying (4 × 4) magic ring array. This fact suggests that phase A follows the bilayer-by-bilayer growth mode. Such a layer-stacked configuration is a structural phase of the Fe−Sb alloy and provides a good template for applications of spintronic devices, for example, magnetic storage and nanoscale biosensor.

To further probe the properties of Fe−Sb superstructures, we performed intensive first-principles calculations to search for the possible atomic structures of the Fe−Sb surface alloy on Sb(111). The calculations show that the Fe atom has a strong tendency to penetrate into the Sb(111) to form a highly coordinated configuration; on the contrary, Sb atom prefers to stay above the substrate with a 3-coordinated structure. On the basis of trying hundreds of initial guesses, we have confirmed two possible 6-fold symmetrical structures for the honeycomb lattice of phase A, as shown in Figure 3 panels a and b, respectively. In the first structure, the topmost atomic layer is constructed by eight Fe and six Sb atoms in each unit cell, so that is called the Fe_8Sb_6 monolayer (Figure 3a). By alternating the Fe and Sb atoms, we can obtain another stable structure, the Fe_6Sb_8 monolayer (Figure 3b). In both structures, seven Fe and Sb atoms form triangle islands with the central atoms located on the lower Sb atoms of the Sb(111) surface layer. Furthermore, in each structure, every two adjacent triangles mirror each other, corresponding to the A and B sublattices in a honeycomb structure,[13] respectively. The Fe−Sb islands in both structures are ∼2.5 Å higher than the Sb(111) surface, and the simulated STM images based on the calculated electron density in the range of the Fermi energy to +0.4 eV (Figure 3c,d) are in great agreement to the high resolution experimental images (Figure 2d).

We further carried out the DFT calculations to figure out the atomic structure of the magic ring above the first Fe−Sb adlayer (bright protrusions in Figure 2e). As mentioned above, the calculation shows that the Fe atom always penetrates into the Sb(111) substrate due to its preference to a high coordination number. As a result, the islands in the second layer can only be composed by pure Sb, which may come from the Sb atoms substituted by Fe atoms and/or out-diffusion from substrate during annealing. On the basis of the Fe_8Sb_6 and Fe_6Sb_8 structures at the first layer, two corresponding structures for the second layer are found by adding 12 and 6 Sb atoms surrounding the hollow sites between the triangle-shaped Fe−Sb atomic array, as demonstrated in Figure 3 panels e and f, respectively. It is noted that in the Fe_8Sb_6 structure, six more Sb atoms were added to stabilize the structure of the first layer (Figure 3e), and hexagonal Sb rings are formed in the second layer of both structures. Such Sb islands are ∼2.0 Å higher than the Fe−Sb atomic arrays, and simulated STM images based on the calculated electron density in the range of the Fermi energy to +0.4 eV (Figure 3g,h) are also perfectly consistent to the experimental observations (Figure 2e,g).

The calculated density of states (DOS) (Figure S3, Supporting Information) reveals that both Fe_8Sb_6 and Fe_6Sb_8 configurations have ferromagnetic metallic electronic structures. Furthermore, the spacial distributions of spin density (purple isosurface in Figure 4) show that the magnetism in the Fe−Sb systems is completely localized on the d bands of the Fe atoms. The calculated magnetic moments (Fe_8Sb_6, 2.53 μB/Fe; Fe_6Sb_8, 2.40 μB/Fe) are higher than that of bulk iron (2.2 μB/Fe), but more close to that of small $Fe_{200-300}$ clusters,[24] due

DOI: 10.1021/acsnano.6b08347
ACS Nano 2017, 11, 2143−2149

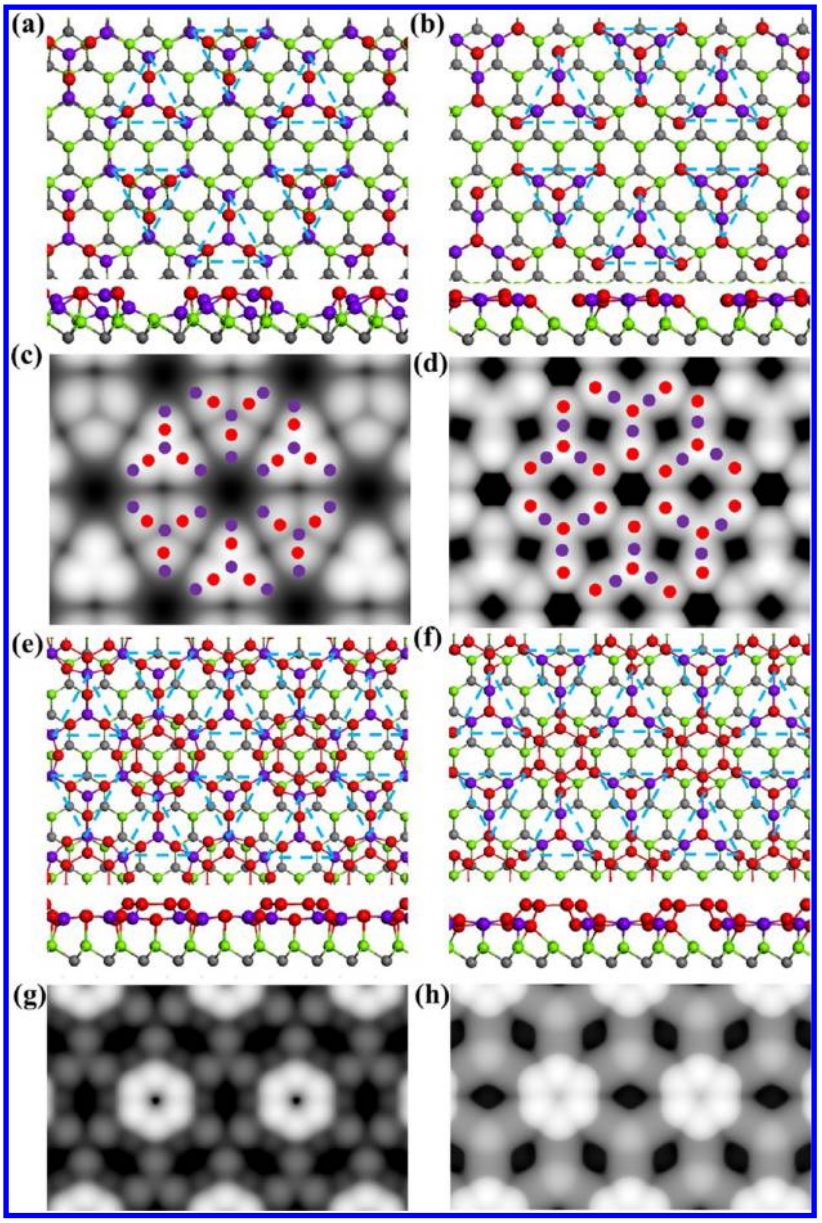

Figure 3. Calculation models and simulated STM images. (a and b) top (upper panel) and side (lower panel) views for Fe_8Sb_6 and Fe_6Sb_8 monolayer structures on Sb(111), respectively. (c and d) Corresponding simulated STM images based on the calculated electron density from Fermi level to +0.4 eV. (e and f) Top (upper panel) and side (lower panel) views for the magic ring structures of the second layer on Fe_8Sb_6 and Fe_6Sb_8 monolayers on Sb(111), respectively. (g and h) Corresponding simulated STM images based on the calculated electron density from Fermi level to +0.4 eV. Purple and red spheres denote to Fe and Sb atoms of the Fe−Sb films, respectively. The green and gray spheres denote the substrate Sb atoms at higher and lower positions, respectively. The blue dash line frames correspond to triangle pattern in the STM image of phase A.

to surface confinement to the delocalization of d electrons in iron. It is surprising that the increased Sb atoms express opposite effects to the magnetism of Fe_8Sb_6 and Fe_6Sb_8 monolayers. The added Sb atoms form Fe−Sb bonds in Fe_8Sb_6, making its magnetic moment reduces to 1.72 μB/Fe; on the contrary, the second-layer Sb ring in Fe_6Sb_8 largely reduces the delocalization of d electrons in Fe, leading to a higher magnetic moment (~2.96 μB/Fe), which is equal to a spin imbalance of *d* bands for the single Fe atom. The identical magnetic moment implies that Fe atoms in bilayer Fe−Sb alloy may possess similar properties to isolated Fe atom, which is potentially applicable as a single atom catalyst.[22,23]

Nanocluster Structure of Fe−Sb Surface Alloy. It is interesting that small amounts of islands with a truncated triangle shape are formed on the Fe/Sb(111) surface, as shown in Figure 5a. Such islands consist of well-ordered protrusions and are very similar to the molecular self-assembly film commonly observed on metal surfaces. It indicates that the superstructure, phase B, can be viewed as identical nanocluster arrays. The height profile taken along the blue line in Figure 5a reveals that phase B has two types of heights relative to the Sb(111) terrace, as shown in Figure 5b. In addition, the right island with a height of about 3.2 Å grows on top of the Sb(111) surface, while the left one dips into the subsurface and exhibits a lower height of about 1.5 Å, implying the mixing characteristic of phase B. The high resolution STM image of phase B indicates that the protrusion seems like three vertex-overlapped equilateral triangles with a mirror-symmetry. Each equilateral

DOI: 10.1021/acsnano.6b08347
ACS Nano 2017, 11, 2143−2149

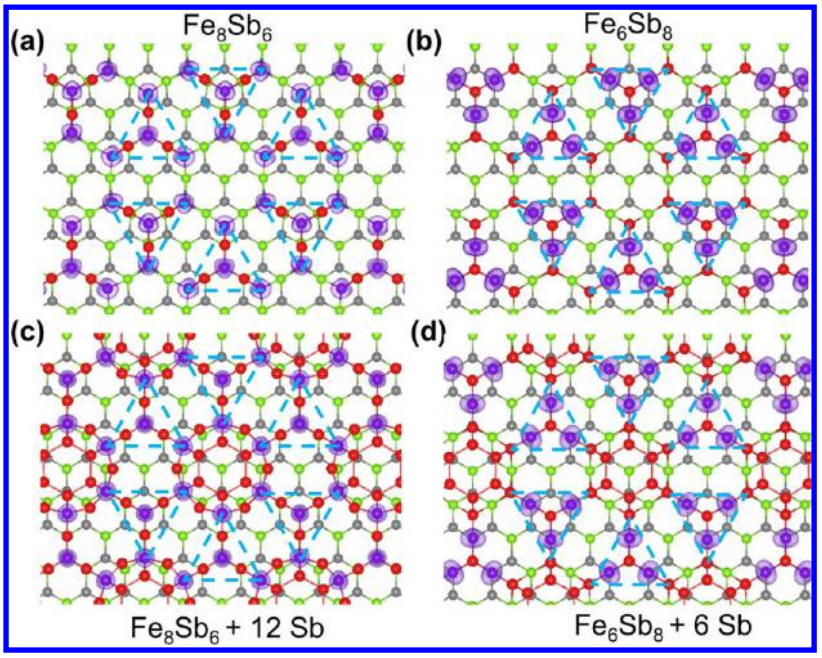

Figure 4. Isosurface plots (isovalue >0.005 e/Å^3) of spin distribution for (a) Fe_8Sb_6 and (b) Fe_6Sb_8 monolayers, as well as the (c) Fe_8Sb_6+12Sb and (d) Fe_6Sb_8+6Sb bilayer structures, respectively. Purple and red spheres denote Fe and Sb atoms in Fe−Sb films, respectively. The green and gray spheres are the substrate Sb atoms at higher and lower positions in the topmost layer of Sb(111). The purple isosurface corresponds to the spin distribution, demonstrating that the magnetism of such systems is completely localized on the Fe atoms.

triangle consists of four atoms where one locates at the center and the others symmetrically distribute at the three vertexes, as shown in Figure 5c,d. The height profile (Figure 5e) taken along one packing array in Figure 5c reveals that the distance of neighboring protrusions is about 1.28 nm, three times that of the lattice constant of the (1 × 1) Sb substrate. Thus, phase B can be expressed as a (3 × 3) reconstruction with respect to the underlying Sb(111)-(1 × 1) surface. To clarify the structure of phase B on Sb(111), the atomic resolution STM image of the substrate and phase B was obtained. In Figure 5f, the upper one corresponds to the configuration of phase B, while the lower part shows the atomic arrangements of the substrate where the dark holes correspond to Sb surface atoms at the positive bias voltage. We can distinguish the adsorption sites and orientations of each atom of phase B *via* superimposing the substrate lattice. The centered atom of each nanocluster resides at the hollow sites of Sb(111). The six corner atoms and the residual three atoms are located at the hollow sites and top sites of Sb(111), respectively.

The first-principles calculations also confirm the 3-fold symmetrical cluster structure that is constructed by three Fe and seven Sb atoms for each nanocluster, as displayed in Figure 5g and Figure S4. Calculations show that the adsorption site with the central Sb above the hollow site of Sb(111) surface is the most stable. The simulated STM image (Figure 5h and Figure S4) is also consistent to the experimental image (Figure 5d). The calculated DOS and spin distribution (Figure S5) demonstrate that the Fe_3Sb_7 cluster possesses a strong ferromagnetic electronic structure. Similar to phase A, the magnetism of phase B is also localized on Fe with a magnetic moment of 1.9 μB/Fe. This configuration provides a method to build spintronics devices on the basis of identical cluster arrays.

Comparison to Co Deposition. Cobalt is another intrinsic magnetic element, potentially applicable in low dimensional materials. On the basis of structural chemistry, it is found that a low coordination number of 3 for Co can be stable due to its d7 electron configuration. On the other hand, at least four electrons are needed for stabilizing the d6 electron configuration, leading to a stronger preference to be highly coordinated for Fe. In our previous work, we studied the cobalt atom deposition on Sb(111) at very low coverage.[25] Different from Fe always penetrating into the substrate, the single adsorbed Co atom adopts alternative metastable states, corresponding to a 3-coordinated protrusion structure above the hollow site of Sb(111) as well as a penetrating adsorption similar to the Fe/Sb(111) structure. In a further experiment, when we increased the coverage of deposited Co atoms, only clusters or disordered structures can be observed on the surface due to the aggregation of Co on Sb(111). To contrast, the characteristic of Fe preference to achieve higher coordination promotes the formation of Fe−Sb alloy instead of Fe islands. This discovery can be conducive when choosing the appropriate transition elements for fabricating the ferromagnetic layers.

CONCLUSIONS

By using STM investigation combined with DFT calculations, we systematically study the atomic structures and magnetism of Fe−Sb surface alloy on the Sb(111) surface. It is found that Sb and Fe atoms can form various alloy structures, including the magnetic honeycomb structure which is a good material for simulating a Haldane model. The high magnetic moment also indicates the Fe atoms in such structure may be good single-atom-site catalysts, and the identical cluster structures can also be applicable in spintronics.

Our results provide a method to fabricate 2D magnetic superstructures on the basis of orthodox magnetic elements that is favorable for promoting practical applications of 2D magnets in the future of device architectures.

DOI: 10.1021/acsnano.6b08347
ACS Nano 2017, 11, 2143−2149

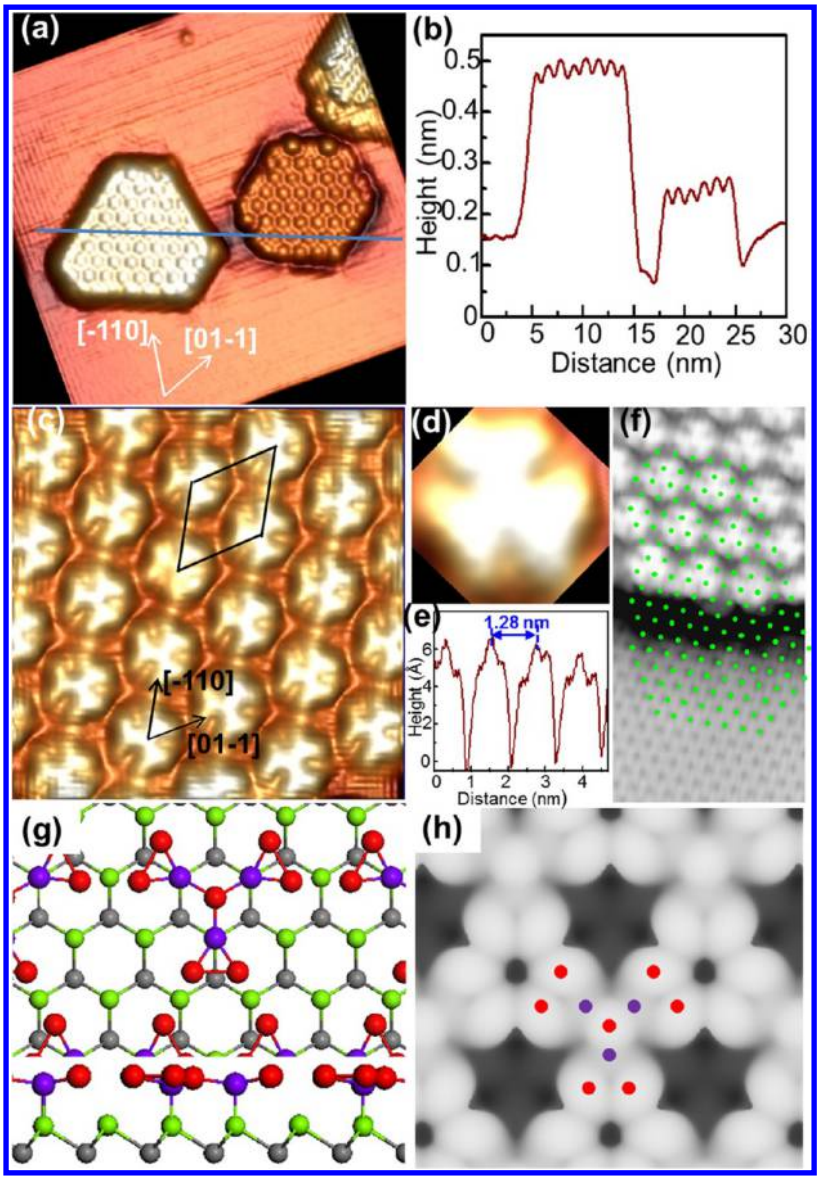

Figure 5. (a) STM topography recorded in the region of phase B (28.2 nm × 28.2 nm). (b) Line profile measured along the blue line in panel a. (c) Atomically resolved STM image recorded on phase B. The unit cell is labeled with a rhombus (5.6 nm × 5.6 nm, U = 1.0 V, I = 0.6 nA). (d) Zoom-in STM image of one nanocluster. (e) A height profile taken along the packing orientation of the nanocluster arrays. (f) Atomically resolved STM image simultaneously recorded on phase B and Sb(111). The Sb(111) lattice (green dots) is superimposed (4.3 nm × 9.7 nm). (g) Top (upper panel) and side (lower panel) views for the Fe_3Sb_7 clusters on Sb(111) substrate. (h) The corresponding STM images simulated by DFT. Purple and red spheres are Fe and Sb atoms of the Fe_3Sb_7 clusters, respectively. The green and gray spheres are the substrate Sb atoms.

METHODS

Experimental Details. The experiments were carried out in an ultrahigh vacuum low temperature STM (Unisoku, Japan) with a base pressure better than 1×10^{-10} Torr. The Sb(111) substrate was *in situ* cleaned by repeated cycles of Ar^+ sputtering and subsequently annealing to about 620 K. The surface quality was checked by STM until the images showed no distinct traces of contaminants. After the Fe rod (2.0 mm diameter, 99.995% purity) equipped in an e-beam evaporator was fully degassed, the samples were prepared by depositing Fe atoms on the Sb(111) substrate at about 500 K. The deposition rate was kept at about 0.1 ML/min (here 1 monolayer refers to the atomic density of an ideal surface of Sb(111)). All STM measurements were performed at liquid nitrogen temperature (about 78 K) with Pt–Ir tips.

Computational Model. First-principles calculations were performed within the framework of density functional theory (DFT) as implemented in Vienna ab Initio Simulation package (VASP).[26] The opt-B88 van der Waals density functional[27] was employed to better describe the interlayer interaction of Fe–Sb alloy, combined with projector-augmented wave (PAW) pseudopotentials as well as a plane-wave basis set with energy cutoff at 300 eV. In our test calculations, it was found that the Fe–Sb adlayer on 2-bilayer-thick and 3-bilayer-thick Sb(111) substrates exhibit identical atomic and electronic structures. Thus, the slab model containing a Fe–Sb superstructure adlayer on a 2-bilayer-thick Sb(111) substrate was used in complicated surface structure calculations, and the vacuum region of >15 Å was applied to reduce interactions between periodic images. All the structures were fully relaxed until the maximum force on each atom is less than 0.04 eV/Å, while the Sb atoms in the bottom bilayer were kept fixed. The first Brillouin zones were sampled by 3 × 3 × 1 and 4 × 4 × 1 Monkhorst–Pack k-mesh for phase A and phase B, respectively.

DOI: 10.1021/acsnano.6b08347
ACS Nano 2017, 11, 2143–2149

ASSOCIATED CONTENT

Supporting Information

The Supporting Information is available free of charge on the ACS Publications website at DOI: 10.1021/acsnano.6b08347.

Figures regarding the sample STM characterization and DFT calculations (PDF)

AUTHOR INFORMATION

Corresponding Authors

*E-mail: huili8@iphy.ac.cn.
*E-mail: gycao@wipm.ac.cn.

ORCID

Yinghui Yu: 0000-0003-3620-2846

Present Address

#School of Physics and Engineering and State Key Laboratory of Optoelectronic Materials and Technologies, Sun Yat-sen University, Xingang Xi Road 135, Guangzhou 510275, China.

Author Contributions

⊥Y.Y. and H.F. contributed equally to this work. L.S. performed the majority of the experiments.

Notes

The authors declare no competing financial interest.

ACKNOWLEDGMENTS

The authors gratefully acknowledge financial support from the NSFC of China with Grant Nos. 11427903 and 11374333.

REFERENCES

(1) Izquierdo, J.; Vega, A.; Balbás, L. C.; Sánchez-Portal, D.; Junquera, J.; Emilio, A.; Soler, J. M.; Ordejón, P. Systematic *ab initio* Study of the Electronic and Magnetic Properties of Different Pure and Mixed Iron Systems. *Phys. Rev. B: Condens. Matter Mater. Phys.* **2000**, *61*, 13639.

(2) Enders, A.; Skomski, R.; Honolka, J. Magnetic Surface Nanostructures. *J. Phys.: Condens. Matter* **2010**, *22*, 433001.

(3) Zhou, J.; Wang, Q.; Sun, Q.; Chen, X. S.; Kawazoe, Y.; Jena, P. Ferromagnetism in Semihydrogenated Graphene Sheet. *Nano Lett.* **2009**, *9*, 3867.

(4) Tsuchiya, T.; Terabe, K.; Aono, M. *In situ* and Non-Volatile Bandgap Tuning of Multilayer Graphene Oxide in an All-Solid-State Electric Double-Layer Transistor. *Adv. Mater.* **2014**, *26*, 1087.

(5) Nair, R. R.; Sepioni, M.; Tsai, I.; Lehtinen, O.; Keinonen, J.; Krasheninnikov, A. V.; Thomson, T.; Geim, A. K.; Grigorieva, I. V. Spin-half Paramagnetism in Graphene Induced by Point Defects. *Nat. Phys.* **2012**, *8*, 199.

(6) Cao, T.; Li, Z.; Louie, S. G. Tunable Magnetism and Half-Metallicity in Hole-Doped Monolayer GaSe. *Phys. Rev. Lett.* **2015**, *114*, 236602.

(7) Wu, S.; Dai, X.; Yu, H.; Fan, H.; Hu, J.; Yao, W. Magnetisms in p-type Monolayer Gallium Chalcogenides (GaSe, GaS), arXiv1409.4733v2. https://arxiv.org/pdf/1409.4733v2.pdf, 2014.

(8) Ma, Y. D.; Dai, Y.; Guo, M.; Niu, C. W.; Zhu, Y. T.; Huang, B. B. Evidence of the Existence of Magnetismin Pristine VX_2 Monolayers (X= S, Se) and Their Strain-Induced Tunable Magnetic Properties. *ACS Nano* **2012**, *6*, 1695.

(9) Xu, K.; Chen, P. Z.; Li, X. L.; Wu, C. Z.; Guo, Y. Q.; Zhao, J. Y.; Wu, X. J.; Xie, Y. Ultrathin Nanosheets of Vanadium Diselenide: A Metallic Two-Dimensional Material With Ferromagnetic Charge-Density-Wave Behavior. *Angew. Chem., Int. Ed.* **2013**, *52*, 10477.

(10) Li, X.; Yang, J. $CrXTe_3$ (X= Si, Ge) Nanosheets: Two Dimensional Intrinsic Ferromagnetic Semiconductors. *J. Mater. Chem. C* **2014**, *2*, 7071.

(11) Williams, T. J.; Aczel, A. A.; Lumsden, M. D.; Nagler, S. E.; Stone, M. B. Magnetic Correlations in the Quasi-Two-Dimensional Semiconducting Ferromagnet $CrSiTe_3$. *Phys. Rev. B: Condens. Matter Mater. Phys.* **2015**, *92*, 144404.

(12) Sivadas, Ni.; Daniels, M. W.; Swendsen, R. H.; Okamoto, S.; Xiao, D. Magnetic Ground State of Semiconducting Transition-Metal Trichalcogenide Monolayers. *Phys. Rev. B: Condens. Matter Mater. Phys.* **2015**, *91*, 235425.

(13) Haldane, F. D. M. Model for a Quantum Hall Effect without Landau Levels: Condensed-Matter Realization of the "Parity Anomaly. *Phys. Rev. Lett.* **1988**, *61*, 2015.

(14) Chang, C.; Zhang, J.; Feng, X.; Shen, J.; Zhang, Z.; Guo, M.; Li, K.; Ou, Y.; Wei, P.; Wang, L.; Ji, Z.; Feng, Y.; ji, S.; Chen, X.; Jia, J.; Dai, X.; Fang, Z.; Zhang, S.; He, K.; Wang, Y.; Lu, L.; Ma, X.; Xue, Q. Experimental Observation of the Quantum Anomalous Hall Effect in a Magnetic Topological Insulator. *Science* **2013**, *340*, 167.

(15) Kane, C. L.; Mele, E. J. Quantum Spin Hall Effect in Graphene. *Phys. Rev. Lett.* **2005**, *95*, 226801.

(16) König, M.; Wiedmann, S.; Brüne, C.; Roth, A.; Buhmann, H.; Molenkamp, L. W.; Qi, X.; Zhang, S. Quantum Spin Hall Insulator State in HgTe Quantum Wells. *Science* **2007**, *318*, 766.

(17) Hsieh, D.; Qian, D.; Wray, L.; Xia, Y.; Hor, Y. S.; Cava, R. J.; Hasan, M. Z. A Topological Dirac Insulator in a Quantum Spin Hall Phase. *Nature* **2008**, *452*, 970.

(18) Hasan, M. Z.; Kane, C. L. Colloquium: Topological Insulators. *Rev. Mod. Phys.* **2010**, *82*, 3045.

(19) Jotzu, G.; Messer, M.; Desbuquois, R.; Lebrat, M.; Uehlinger, T.; Greif, D.; Esslinger, T. Experimental Realization of the Topological Haldane Model with Ultracold Fermions. *Nature* **2014**, *515*, 237.

(20) Li, L.; Wang, Y.; Xie, S.; Li, X.; Wang, Y.; Wu, R.; Sun, H.; Zhang, S.; Gao, H. Two-Dimensional Transition Metal Honeycomb Realized: Hf on Ir(111). *Nano Lett.* **2013**, *13*, 4671.

(21) Zhao, J.; Deng, Q.; Bachmatiuk, A.; Sandeep, G.; Popov, A.; Eckert, J.; Rümmeli, M. H. Free-Standing Single-Atom-Thick Iron Membranes Suspended in Graphene Pores. *Science* **2014**, *343*, 1228.

(22) Guo, X. G.; Fang, G. Z.; Li, G.; Ma, H.; Fan, H. J.; Yu, L.; Ma, C.; Wu, X.; Deng, D. H.; Wei, M. M.; Tan, D. L.; Si, R.; Zhang, S.; Li, J. Q.; Sun, L. T.; Tang, Z. C.; Pan, X. L.; Bao, X. H. Reaching the Magnetic Anisotropy Limit of a 3d Metal Atom. *Science* **2014**, *344*, 616.

(23) Deng, D.; Chen, X.; Yu, L.; Wu, X.; Liu, Q.; Liu, Y.; Yang, H.; Tian, H.; Hu, Y.; Du, P.; Si, R.; Wang, J.; Cui, X.; Li, H.; Xiao, J.; Xu, T.; Deng, J.; Yang, F.; Duchesne, P. N.; Zhang, P.; Zhou, J.; Sun, L.; Li, J.; Pan, X.; Bao, X. A Single Iron Site Confined in a Graphene Matrix for the Catalytic Oxidation of Benzene at Room Temperature. *Sci. Adv.* **2015**, *1*, e1500462.

(24) Billas, I. M. L.; Châtelain, A.; de Heer, W. A. Magnetism from the Atom to the Bulk in Iron, Cobalt, and Nickel Clusters. *Science* **1994**, *265*, 1682.

(25) Yu, Y. H.; She, L. M.; Fu, H. X.; Huang, M.; Li, H.; Meng, S.; Cao, G. Y. Kondo Effect Mediated Topological Protection: Co on Sb(111). *ACS Nano* **2014**, *8*, 11576.

(26) Kresse, G.; Furthmüller, J. Efficient Iterative Schemes for Ab Initio Total-Energy Calculations Using a Plane-Wave Basis Set. *Phys. Rev. B: Condens. Matter Mater. Phys.* **1996**, *54*, 11169.

(27) Klimeš, J.; Bowler, D. R.; Michaelides, A. Van der Waals Density Functionals Applied to Solids. *Phys. Rev. B: Condens. Matter Mater. Phys.* **2011**, *83*, 195131.

DOI: 10.1021/acsnano.6b08347
ACS Nano 2017, 11, 2143–2149